iJET EXPLORE International Journal of Engineering & Technology
CENTRE OF PROFESSIONAL RESEARCH PUBLICATIONS
ISSN 2049-3444

International Journal of Engineering and Technology Volume 2 No. 10, October, 2012

Characteristics of Commercially Pure Aluminum 1020 after Simple Compression Process

S. T. Adedokun[1], T. A. Fashanu[2], S. Oyebanji[3]
[1]Department of Mechanical Engineering, Covenant University, Canaanland, Ota, Nigeria
[2]Department of Systems, University of Lagos, Akoka-Yaba, Lagos, Nigeria
[3]Department of Mechanical Engineering, Alabama State University, Auburn, AL, USA

ABSTRACT

Deformation of a miniaturized aluminum specimens were carried out experimentally using a simple compression test. This test was used to verify the simulation technique based on the crystal plasticity model with which grain-by-grain deformation behavior can be anticipated. 99.99% polycrystalline aluminum cubes with dimensions of 3 mm × 3 mm × 3 mm is tested. Application of consecutive heat treatments produced an average grain size in the aluminum specimens of 1 – 3 mm. The specimens used in this study were classified into two types: the miniaturized specimens (supposedly with a single grain, *type1*) and the specimens composed of several grains (*type2*). Electron backscattered diffraction (EBSD) system was used to quantify the grain orientations of the heavily deformed specimens used. The resultant deformations of the *type1* specimens are then compared with the calculations based on the crystal plasticity. For the *type2* specimens, finite element method (FEM) using the crystal plasticity material model is adopted to predict the complicated grain-by-grain deformations. The similarity between the experimental observations and the FEM predictions is compared in a qualitative manner.

Keywords: *Aluminum 1020, Simple compression, Single grain, EBSD, Finite element method*

1. INTRODUCTION

With the advancement in technology, miniaturization of products and parts has become an essential component of the manufacturing process. Some of the features of these miniature products are miniaturized to the size of metal grains. In such case, the deformation behavior of miniature products is different from that of macro size products [Tiesler et al., 2002]. This deformation behavior is assumed to be affected by the ratio of the grain size and the feature size because the grain deformation strongly depends on the crystallographic orientation of the individual grain. A single crystal deforms anisotropically along the slip system, which is determined by the grain orientation. A polycrystal composed of several grains deforms heterogeneously over grain-by-grain as a result of the anisotropic deformations of the individual grains. The grain-by-grain heterogeneity of polycrystal deformation becomes important as the feature size becomes as small as the size of a grain.

Experimental and theoretical investigations have been conducted to observe and predict such deformation behaviors. Some investigations examined the deformation behavior of a single crystal based on the relation between grain orientation and crystal deformation [Moke and Maddin, 1956], [Humphreys and Ardakani, 1994], [Liu et al. 1998], [Castaing et al., 1998], [Akef and Driver, 1991] and [Jasienski et al., 1995], while others examined the polycrystalline cases [Panchanadeeswaran et al., 1996], [Bhattacharyya et al., 2001], [Kim, 2001], [Liu, 1998] and [Beaudoin et al., 2000]. However, these investigations are focused on the texture changes of the grains rather than the grain-by-grain deformation of the grain aggregate. To fully understand the behavior of miniaturized metallic parts under the metal forming operations, we need a precise experimental observation of the deformation of specimens with a few grains.

In this paper, we showed the grain-by-grain deformation behavior of aluminum specimens by conducting a simple compression test. 99.99% pure polycrystalline aluminum cubes with dimensions of 3 mm × 3 mm × 3 mm were used. The specimens were classified into two types: the specimens predominated by a single grain (*type1*) and the specimens composed of several grains (*type2*). The initial crystallographic orientations of the individual grains on the specimen surface, which were measured by the EBSD system, were used as input data for the crystal plasticity model calculation [Kim and Oh, 2003]. The surface profiles of the deformed specimens were measured by an optical non-contact three-dimensional profiler, ACCURA2000. CAD data were obtained using the measured surface profiles. The validity of the FEM technique based on the crystal plasticity model as a predicting tool for the grain-by-grain deformation behavior was examined by comparing the CAD data with the FEM prediction.

2. CRYSTAL PLASTICITY

Since the pioneering work by Taylor and Elam, 1923 and Taylor and Elam, 1925, many studies on crystal plasticity

have been conducted to predict the overall response of polycrystalline metals: Asaro and Needleman, 1985; Mathur and Dawson, 1989; Mathur and Dawson, 1990; Beaudoin et al., 1996; and Kalidindi and Anand, 1993. Recently, the strain gradient effect due to the geometrically necessary dislocation has been considered in the formulation for crystalline materials: Shu and Fleck, 1999; Acharya and Bassani, 2000; Beaudoin et al., 2000.

Kim and Oh, 2003 developed a strain gradient type formulation to be used for theoretically estimating the grain-by-grain deformation, which would be compared with the experimental observations conducted in the current investigation as shown below. Essential features of the formulation are as follows.

The resolved shear stress $\tau^{(\alpha)}$ on the α-th slip system of the crystalline material is calculated by

$$\tau^{(\alpha)} = s_i^{(\alpha)} \sigma_{ij} n_j^{(\alpha)} \quad \text{(no summation on } \alpha\text{)} \tag{1}$$

where σ_{ij} is the externally applied stress, $s_i^{(\alpha)}$ slip direction and $n_j^{(\alpha)}$ is the slip plane normal vector of the α-th slip system, respectively.

If the resolved shear stress $\tau^{(\alpha)}$ is determined from Eq. (1), the resolved shear strain-rate $\dot{\gamma}^{(\alpha)}$ on the α-th slip system can be determined from the following rate-sensitive constitutive equation for the slip system.

$$\dot{\gamma}^{(\alpha)} = \dot{\gamma}_0^{(\alpha)} \left(\frac{\tau^{(\alpha)}}{\tau_R^{(\alpha)}} \right) \left| \frac{\tau^{(\alpha)}}{\tau_R^{(\alpha)}} \right|^{\frac{1}{m}-1} \tag{2}$$

where $\dot{\gamma}_0^{(\alpha)}$ is the reference shear strain-rate on the α-th slip system, $\tau_R^{(\alpha)}$ the reference shear stress on the α-th slip system and m is the rate-sensitivity parameter.

Then the macroscopic strain-rate $\dot{\varepsilon}_{ij}$ is given by

$$\dot{\varepsilon}_{ij} = \sum_{\alpha=1}^{N} \dot{\gamma}^{(\alpha)} s_i^{(\alpha)} n_j^{(\alpha)} \tag{3}$$

where N is the number of active slip system. In the rate-sensitive constitutive modeling for the face-centered cubic (fcc) material, the value of N becomes 12.

In addition to the stress and the strain-rate, the couple stress and the curvature-rate are included in the formulation through the virtual work-rate principle given by

$$\int_V \sigma_{ij} \delta \dot{\varepsilon}_{ij} \, dV + \int_V \mu_{pk} \delta \dot{\chi}_{kp} \, dV = \int_S F_i \partial v_i \, dS + \int_S M_k \delta \omega_k \, dS \tag{4}$$

where μ_{ij} is the couple stress and $\dot{\chi}_{kp}$ the curvature-rate. F_i is the traction, v_i the velocity, M_i the couple traction and ω_i is the angular velocity on the boundary surface, respectively.

To formulate the constitutive equation between the couple stress and the curvature-rate, the following equation is used as an approximation:

$$\frac{\mu_{ij}}{\bar{\mu}} = L \frac{\dot{\chi}_{ij}}{\bar{\chi}} \tag{5}$$

In Eq. (5), $\bar{\mu}$ is defined as an effective couple stress, $\bar{\chi}$ an effective spatial gradient of the angular velocity and L is a proportional constant that is set to be 1 for convenience.

The hardening equation for the couple stress is expressed as:

$$\bar{\mu} = C \bar{\chi} \tag{6}$$

where C is defined as the hardening coefficient of the couple stress.

For more detailed information of the formulation and the material properties used, refer to Kim and Oh, 2003.

Based on the above formulation, FEM calculation was conducted to predict the large deformation behavior of single- and poly-crystalline metallic specimen.

3. EXPERIMENTAL PROCEDURE

The experimental procedure of the present research is briefly shown in Fig. 1. 99.99% pure aluminum of the fcc crystal structure was used as raw material. The grain size of the raw aluminum specimen was about 100–200 μm in diameter. This grain size was too small to make several mm-sized specimens composed of a few grains. Therefore, we grew the grain to about 1–3 mm in diameter by consecutive heat treatments at temperatures of 450–500 °C (±30 °C) for several days. From the annealed aluminum material, cube-shaped specimens with a dimension of 3 mm × 3 mm × 3 mm were made by a milling process. To measure the surface grain

orientations, the EBSD system was used. For the surface treatment before the EBSD measurement, the specimens were mounted inside a polyester resin, and the surfaces were polished by a 1000 meshed polishing paper and etched with 20–30% NaOH solution at room temperature. Then, the surface grain orientations of each specimen were measured for four side surfaces that can be observed during the compression test. After the EBSD measurement, the specimens were compressed between flat dies to 70% of the initial height by INSTRON5565. The simple compression test was carried out at 0.1 mm/min ram velocity and room temperature.

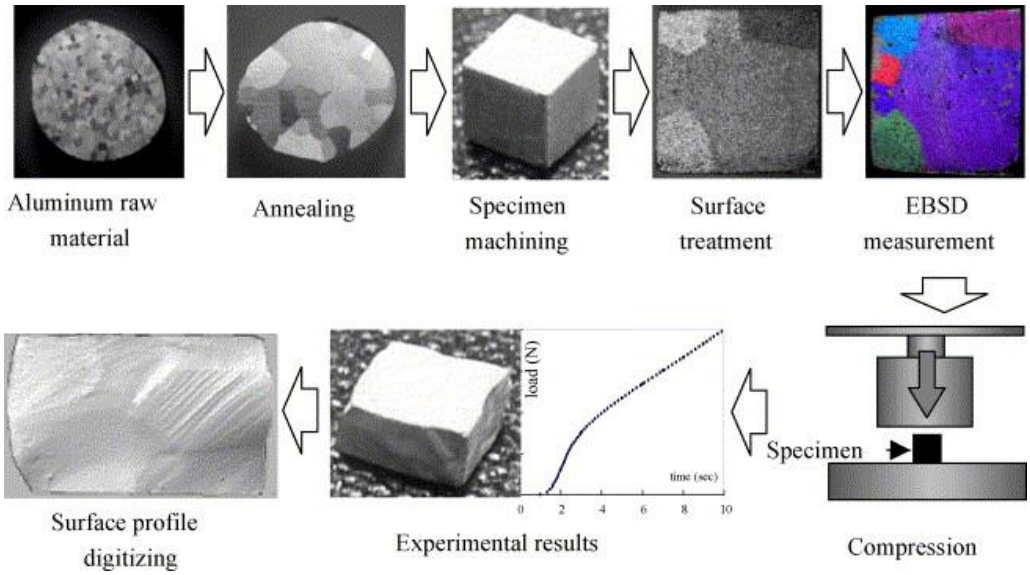

Fig. 1: Experimental procedure

4. EXPERIMENTAL RESULTS

4.1 EBSD Measurement

Fig. 2 shows the results from the EBSD measurement. The different colors indicate the different grain orientations. By the surface grain information, the specimens could be classified into two types. *Type1* specimen includes the specimens predominated by a single grain and *type2* specimen includes the specimens composed of several grains. As the EBSD system measures only the surface grain, information of the inner grain is impossible to obtain without slicing the specimen. However, the sliced specimen cannot be used for the compression test. The small grain in the *type1* specimen shown in Fig. 2 may occupy some portion of the interior of the specimen. However, it does not seem to occupy a large portion. This is confirmed by the compression test results in which the *type1* specimens have the parallel-piped deformed shapes. Therefore, the specimens were classified by the surface grain information only.

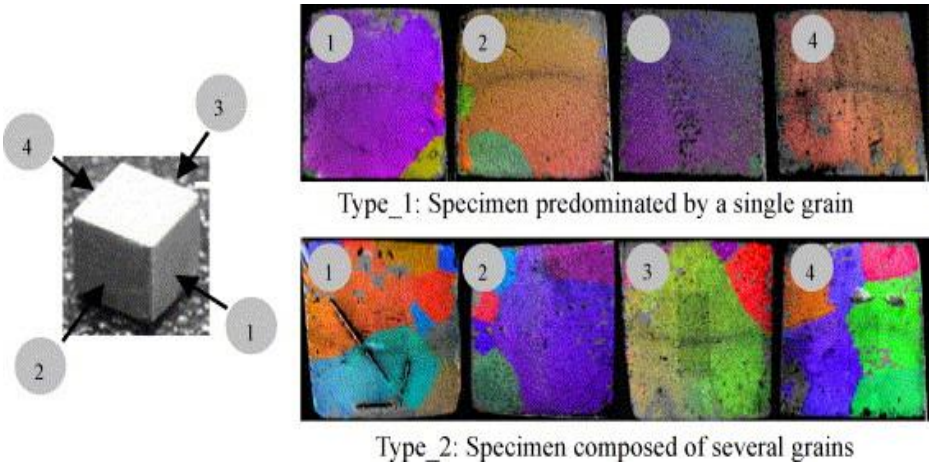

Fig. 2: Electron Back Scattered Diffraction Measurement Result

4.2 Type1: Specimen Predominated by a Single Grain

Fig. 3 shows two examples of the compressed shapes of the *type1* specimens. Each surface remains almost flat even though the sides were tilted arbitrarily due to the anisotropic deformation by the crystalline slip. The slip lines and slip bands are seen to develop in almost the same direction on each side. The specimen in Fig. 3 (a) shows a stronger anisotropic deformation than that in Fig. 3(b) because the predominant grain in Fig. 3(a) becomes deformed more anisotropically than that in Fig. 3(b).

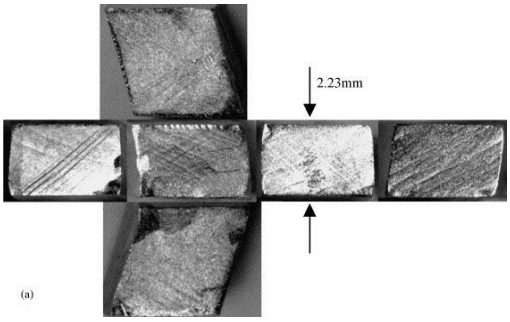

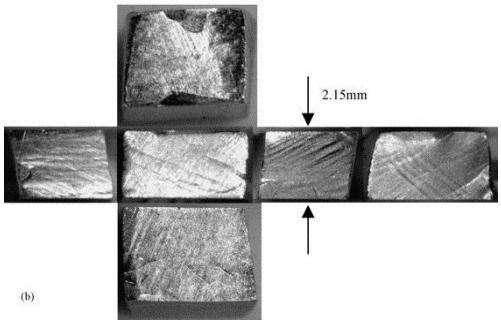

Fig. 3: Deformed shape of the *type1* specimens: (a) 23.1% compression and (b) 26.9% compression

The different levels of strong anisotropic deformation behavior exhibited by the *type1* specimens can be explained based on the crystal plasticity theory. Fig. 4 shows the schematic diagram of the plane strain compression for the cubic single crystal with the spatial coordinate system and the initial orientation of the embedded crystal lattice. Shear strain, γ, and normal strain, ε, were used to describe the deformation as shown in Fig. 5.

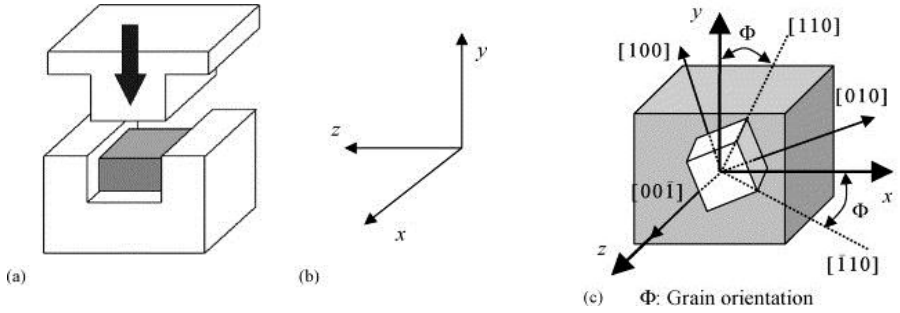

Fig. 4: (a) Schematic diagram of the plane strain compression of single crystal, (b) spatial coordinate system and (c) initial orientation of embedded crystal lattice

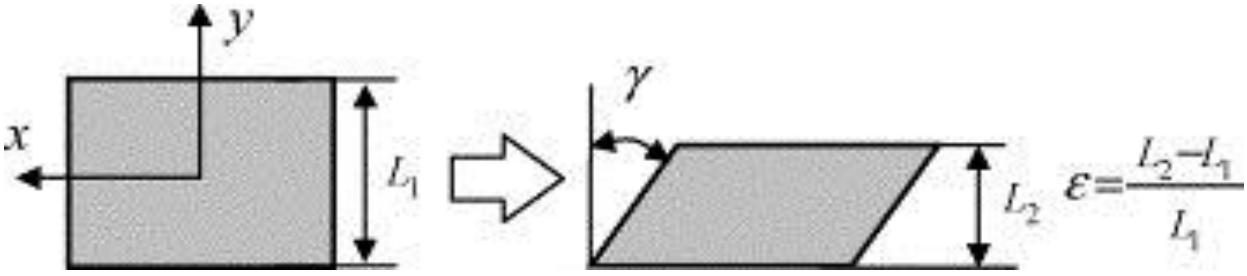

Fig. 5: Definition of shear strain (γ) and normal strain (ε)

The deformation of specimens with different initial grain orientations during the plane strain compression was calculated by applying the crystal plasticity theory. The initial deformation is shown in Fig. 6, where *m* is the rate-sensitivity parameter of the rate-sensitive crystal model. The vertical axis in Fig. 6(a) is the ratio of shear to normal strain, which indicates how much the specimen shears per unit amount of reduction. Therefore, Fig. 6(a) shows that the deformed shape strongly depends on the grain orientation. Likewise Fig. 6(b) shows that the load strongly depends on the grain orientation.

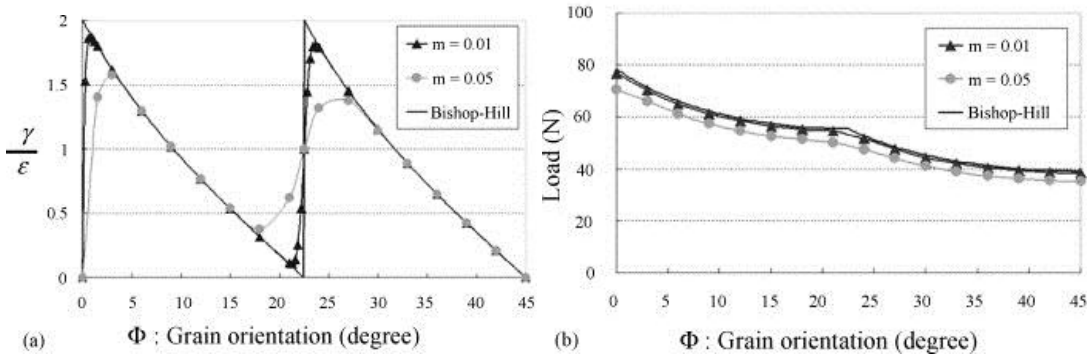

Fig. 6: Prediction by crystal plasticity (a) orientation dependency of deformation and (b) orientation dependency of load

The three-dimensional theoretical prediction by the crystal plasticity model was compared with the experimental compression result as shown in Fig. 7. The crystal plasticity model used the predominant grain orientation measured by the EBSD as the initial orientation of the cubic single crystal model. The theoretically calculated result in Fig. 7(b) was similar to the experimentally observed result in Fig. 7(c) for the shear strain values as well as the overall deformation tendency. The small discrepancy between the theoretical and the experimental result seems to be attributed to the errors related to the material properties such as crystal modeling, friction coefficient, specimen preparation, EBSD measurement and so on. However, these results show that the calculation by the crystal plasticity model is reasonable to predict the deformation behavior of the *type1* specimen.

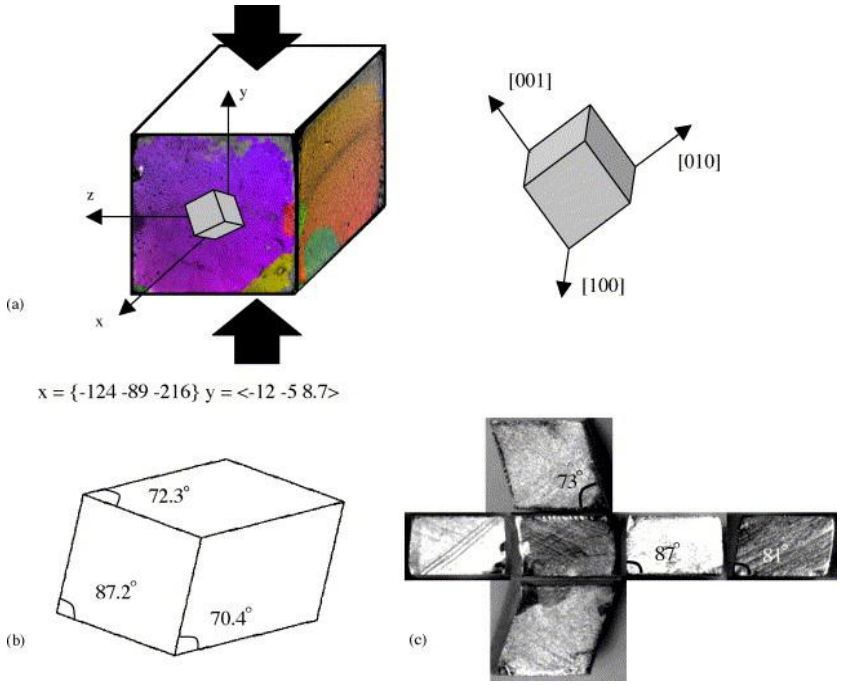

Fig. 7: Comparison between experimental result and theoretical prediction: (a) initial grain orientation measured by EBSD system, (b) crystal plasticity prediction and (c) experimental result.

4.3 Type2: Specimen Composed of Several Grains

Fig. 8 shows two examples of the compressed shapes of *type2* specimens. We can see irregularly curved surfaces, which are in contrast to the *type1* specimens. Especially around the grain boundaries, we can see severely curved surfaces. Various slip lines and slip bands are also observed. It is believed that each grain of the specimen had tried to follow the deformation mode as determined by the crystalline slip under the grain-to-grain interaction, and this consequently resulted in curved surfaces to develop not only on the inside of the grains but also at the grain boundaries.

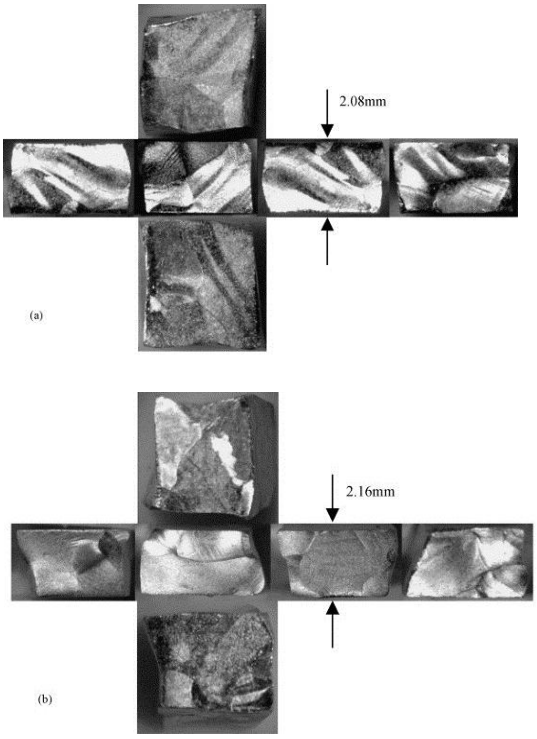

Fig. 8: Deformed shape of *type1* specimens: (a) 27.5% compression and (b) 31.9% compression

The crystal plasticity model was expected to predict the severely curved and distorted surface shapes as the model could predict the deformation for the *type1* specimen. However, in the *type2* specimen case, a numerical simulation tool such as FEM was used to predict the complicated deformation behavior of the grain aggregate. For more detailed information on the FEM technique, refer to Kim and Oh, 2003.

The plane strain compression was simulated for the bi-crystal cases. The initial grain orientations and the simulated results are shown in Fig. 9. The FEM calculation showed a prediction of different deformation shapes for the different initial grain orientations. Although the FEM simulation, itself, cannot predict the differently developed slip lines and slip bands, the FEM simulation using the crystal plasticity model can explain the severely distorted surface shapes. In principle, the three-dimensional deformation of polycrystalline specimens can be calculated by the current crystal plasticity model. However, the FEM prediction of the deformations of the *type2* specimens could not be obtained in the present investigation because of the limitation of EBSD measurement as described above. That is, the entire grain information necessary for the FEM calculation of the *type2* specimen could not be obtained without damaging the initial specimen.

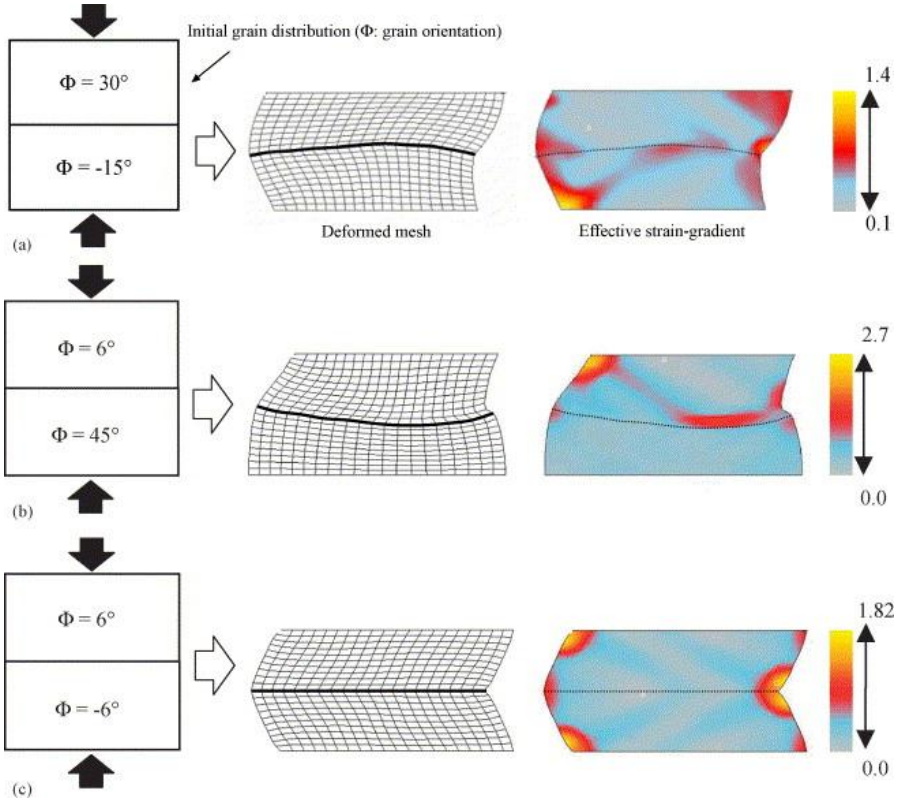

Fig. 9: Plane strain compression of bi-crystal: (a) upper grain orientation = 30° and lower grain orientation = −15°, (b) upper grain orientation = 6° and lower grain orientation = 45° and (c) upper grain orientation = 6° and lower grain orientation = −6°.

Instead of measuring the interior grain information, the surfaces of the deformed specimen were digitized by ACCURA2000, and these digitized data were converted to the CAD data. The resulting data describes the deformations of the specimens quantitatively and can be utilized to validate the three-dimensional FEM predictions of the grain-by-grain deformations in the further investigation. Fig. 10(a) shows the four sides of the deformed specimen and Fig. 10(b) shows the CAD representation of the corresponding surfaces. As the optical profiler could not measure the stiff slope, some of the parts are not properly represented by the CAD data.

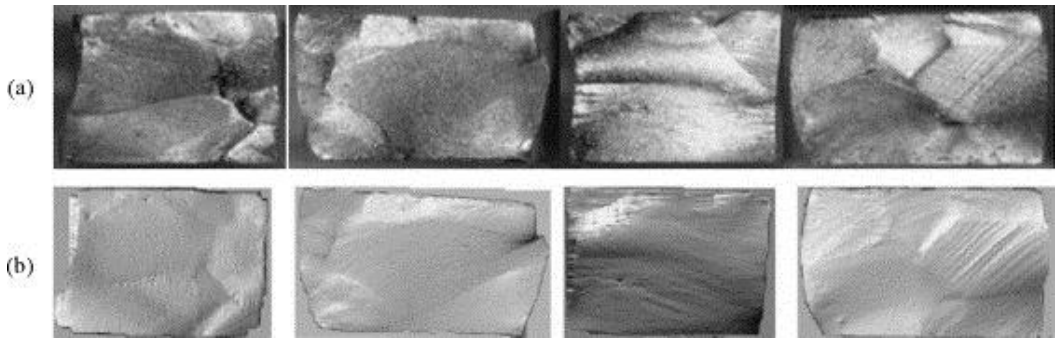

Fig. 10: Surface profile digitizing: (a) real surface shapes and (b) CAD representation

Fig. 11(a) shows the digitized three-dimensional surface profile of the 22.4% compressed specimen. The grains of the specimen were initially about 1 mm in size. Each line of Fig. 11(b) indicates the line profile along the corresponding line marked in Fig. 11(a). R_{PV}, which represents the distance from peak to valley of the surface profile was measured to compare the experimental deformation with the FEM prediction. From the measurements for all *type2* specimen, we obtained an average value of about 300 μm for R_{PV}. On the other hand, R_{PV} for the FEM prediction using the bi-crystal model was about 200 μm as shown in Fig. 9. The initial bi-crystal model in Fig. 9 was composed of two grains with dimensions of 0.5 mm × 1 mm × 1 mm. Although the experimental results were not compared with the FEM calculations using the actual polycrystal data that is concerned with the inner grains as well as the surface grains, the similarity of the average R_{PV} values imply that the FEM technique by the crystal plasticity model reasonably describes the grain-by-grain deformation behavior of the several grained specimens.

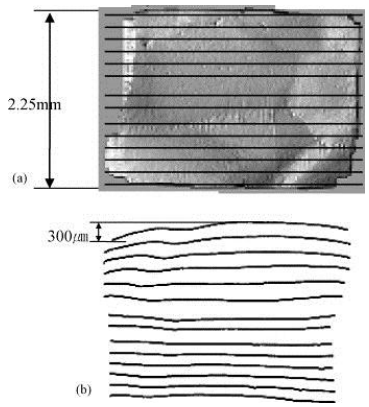

Fig. 11: (a) Digitized surface profile and (b) line surface profile

Fig. 12(a) shows the flow stress curves of the simple compression test for both *type1* and *type2* specimens. The dotted lines indicate the flow stress curves of *type1* specimens and solid lines indicate those of *type2* specimens. The flow stresses of *type2* specimens can be seen to be almost always higher than those of *type1*. This hardening enhancement for the case of *type2* specimens is the result of the grain-to-grain interaction. The flow stress curves of the *type1* specimens are different from each other because the grain orientations of the predominant grains of the specimens are different. The flow stress difference caused by the grain orientation difference was predicted by the calculation using the crystal plasticity model for the plane strain compression of single crystal specimens as shown in Fig. 12(b).

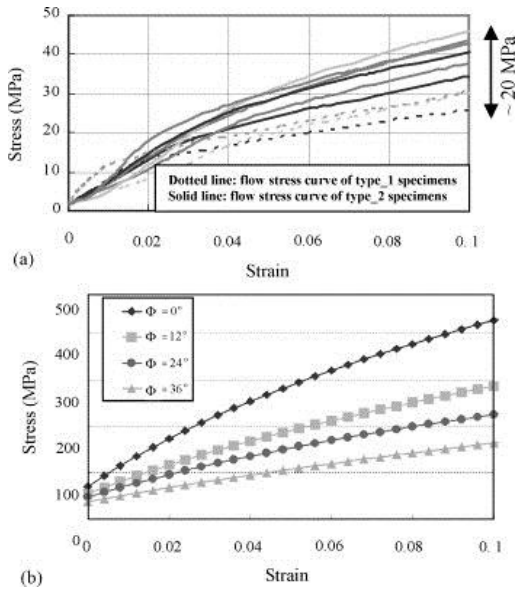

Fig. 12: Stress–strain curve: (a) experimental result and (b) plane strain compression result of single crystal

5. CONCLUSIONS

To verify the performance of the simulation technique using the crystal plasticity model for the grain-by-grain deformation prediction, we gathered experimental data on the deformations of the aluminum specimens with a few grains. Surface grain orientations of the cube-shaped specimen were obtained by the EBSD system. The deformation and the load behavior of *type1* specimens were found to be dependent on the crystalline orientation of the predominant grain. The shear strain and the deformation tendency obtained from the crystal plasticity model calculation for single crystals were similar to the experimental results of the *type1* specimens. On the other hand, the deformations of the *type2* specimens showed considerably curved and distorted surface profiles, especially around the grain boundaries. Such irregularly curved surfaces are attributed to the anisotropic deformations of individual grains resulting from the interaction with the surrounding grains. In addition, we found that the FEM predictions for the plane strain compression of the bi-crystal model were qualitatively similar to the experimental deformations of the *type2* specimens.

In the present investigation, we examined how the metallic specimens with a few grains undergo deformation under the metal forming operations by observing the grain-by-grain deformations. The experimental data validates the FEM technique using the crystal plasticity model for the grain-by-grain deformation prediction. If a measuring technique for the entire grain information, including the inner grains of the initial specimen, is developed in the future, the proposed FEM technique will be useful in predicting the actual polycrystalline specimen deformation.

REFERENCES

[1] A. Acharya and J.L. Bassani (2000) 'Lattice incompatibility and a gradient theory of crystal plasticity' *Journal of the Mechanics and Physics of Solids* **48**, Pp. 1565–1595.

[2] A. Akef and J.H. Driver (1991) 'Orientation splitting of cube-oriented face-centered cubic crystals in plane strain compression' *Material Science & Engineering* **A132**, Pp. 245–255.

[3] R.J. Asaro and A. Needleman (1985) 'Texture development and strain hardening in rate dependent polycrystals' *Acta Metallurgica* **33**, Pp. 923–953.

[4] A.J. Beaudoin, A. Acharya, S.R. Chen, E.A. Korzekwa and M.G. Stout (2000) 'Consideration of grain-size effect and kinetics in the plastic deformation of metal polycrystals' *Acta Materialia* **48**, Pp. 3409–3423.

[5] A.J. Beaudoin, J.D. Bryant, P.R. Dawson and D.P. Mika (1996) 'Incorporating crystallographic texture in finite element simulations of sheet forming' *Numisheet* **96**, Pp. 17–24.

[6] A. Bhattacharyya, E. El-Danaf, S.R. Kalidindi and R.D. Doherty (2001) 'Evolution of grain-scale microstructure during large strain simple compression of polycrystalline aluminum with quasi-columnar grains: OIM measurements and numerical simulations' *International Journal of Plasticity.* **17**, Pp. 861–883.

[7] J. Castaing, T.E. Mitchell and A.D. Rodriguez (1998) 'Evolution of specimen shape for uniaxial compression of single crystals' *Scripta Materialia* **38** (1), Pp. 45–51.

[8] F.J. Humphreys and M.G. Ardakani (1994) 'The deformation of particle-containing aluminum single crystals' *Acta Metallurgica* **42**, Pp. 749–761.

[9] Z. Jasienski, H. Paul, A. Piatkowski and A. Litwora (1995) 'Microstructure and texture of copper single crystal of (1 1 2)[111] orientation undergoing channel-die compression at 77 K, *Journal of Materials Processing & Technology.* **53** (1995), pp. 187–194.

[10] S.R. Kalidindi and L. Anand (1993) 'Large deformation simple compression of a copper single crystal' *Metalurgica Transanctions* **24A**, Pp. 989–992.

[11] K.-H. Kim (2001) 'Grain by grain deformation behavior of pure aluminum during simple compression' Master Theses, Seoul National University.

[12] H.-K. Kim and S.-I. Oh (2003) 'Finite element analysis of grain-by-grain deformation by crystal plasticity with couple stress' *International Journal of Plasticity* **19**, Pp. 1245–1270.

[13] Q. Liu, D. Juul Jensen and N. Hansen (1998) 'Effect of grain orientation on deformation structure in cold-rolled polycrystalline aluminum' *Acta Materialia* **46** (16), Pp. 5819–5838.

[14] K.K. Mathur and P.R. Dawson (1989) 'On modeling the development of crystallographic texture in bulk forming processes' *International Journal of Plasticity* **5**, Pp. 67–94.

[15] K.K. Mathur and P.R. Dawson (1990) 'Texture development during wire drawing' *ASME Journal of Engineering Material Technology* **112**, Pp. 292–297.

[16] J.H. Moke and R. Maddin (1956) 'The deformation of molybdenum single crystals in compression' Journal of the Mechanics and Physics of Solids **5**,Pp. 26–36.

[17] S. Panchanadeeswaran, R.D. Doherty and R. Becker (1996) 'Direct observation of orientation change by channel die compression of polycrystalline aluminum-use of a split sample' *Acta Materialia* **44** (3), Pp. 1233–1262.

[18] J.Y. Shu and N.A. Fleck (1999) 'Strain gradient crystal plasticity: size-dependent deformation of bicrystals' *Journal of the Mechanics and Physics of Solids* **47**, Pp. 297–324.

[19] G.I. Taylor and C.F. Elam (1923) 'The distortion of an aluminum crystal during a tensile test', *Proceedings Royal Society London* **A102**, Pp. 643–667.

[20] G.I. Taylor and C.F. Elam (1925) 'The plastic extension and fracture of aluminum crystals' *Proceedings Royal Society London* **A108**, Pp. 28–51.

[21] N. Tiesler, U. Engel and M. Geiger (2002) 'Basic research on cold forging of microparts' *Proceedings of 7th ICTP 1* (2002), pp. 379–384.

